Vibrational Dynamics of $LiBH_4$ by Infrared Pump−Probe and 2D Spectroscopy

Esben Ravn Andresen,[†] Robin Gremaud,[‡] Andreas Borgschulte,[‡] Anibal Javier Ramirez-Cuesta,[§] Andreas Züttel,[‡] and Peter Hamm*[,†]

Physikalisch-Chemisches Institut, Universität Zürich, Winterthurerstrasse 190, CH-8057 Zürich, Switzerland, Empa, Swiss Federal Laboratories for Materials Testing and Research, Hydrogen & Energy, Überlandstrasse 129, CH-8600 Dübendorf, Switzerland, and ISIS Facility, Rutherford Appleton Laboratory, Chilton, Didcot, Oxon OX11 0QX, U.K.

Received: August 11, 2009; Revised Manuscript Received: September 11, 2009

Employing femtosecond IR pump−probe and 2D spectroscopy, we measure the vibrational dynamics of $LiBH_4$ and several of its deuterium isotopomers. We find that the vibrational lifetime of various BH and BD stretching modes uniformly is ≈1.5 ps for all $BH_{4-x}D_x^-$ units ($0 \le x \le 4$). Subsequently, vibrational energy cascades down through BH and BD bending, facilitated by a strong Fermi resonance, into external (librational and translational) modes with a 3 ps time constant. Final thermalization of the energy is completed in about 100 ps. The vibrational spectra are purely homogeneously broadened indicating low inhomogeneity due to static disorder. We furthermore measured the anharmonic constants of various modes, which sets the benchmark for future *ab initio* calculations, and completed the first FTIR assignment of the stretching vibrations for the five $BH_{4-x}D_x^-$ units.

Introduction

Complex hydrides are promising candidates for hydrogen storage applications.[1] Among them, $LiBH_4$,[2] an ionic solid consisting of Li^+ ions and BH_4^- ions, has one of the highest known gravimetric hydrogen densities of 18 mass % and volumetric hydrogen density of 121 kg m^{-3}. Despite considerable research effort, the conditions for hydrogen uptake and release by $LiBH_4$ remain harsh.[3−5] A better understanding of the hydrogen dynamics is needed to improve the (de)hydrogenation reversibility and kinetics of the system by, e.g., adding catalysts or additives[6] or substituting cations or anions.[7,8] Hydrogen dynamics in $LiBH_4$ comprises long-range lattice phonon modes and diffusion as well as localized motions like BH_4^- vibrations, librations, or rotations. The various motions are characterized by their specific length and time scales. At the shortest and fastest end is vibrational dynamics, hitherto studied by infrared spectroscopy,[9] inelastic neutron,[10] and Raman scattering.[11−13] Besides vibrations, quasifree rotations of the BH_4^- unit are possible above the low-temperature- (LT) to high-temperature (HT) phase transition temperature at 380 K, and are accessible by nuclear magnetic resonance (NMR)[14] and quasielastic neutron spectroscopy.[15] A necessary step in the hydrogen ab/desorption process is long-range hydrogen diffusion. No H-swapping between BH_4^- units could be observed by NMR on a time scale of milliseconds below melting, suggesting that H transport in $LiBH_4$ is dominated by BH_4^- diffusion in the solid,[16] like in the liquid phase.[17] However, Raman scattering measurements on H/D isotope-scrambled $LiBH_4$ showed that even though the BH_4^- unit is very stable, single deuterium atoms are successively exchanged in the complex BH_4^- units at temperatures below melting.[18] The H/D exchange occurs most probably at low-concentration defects or at the surface, as the bulk-sensitive NMR technique could not evidence atomic H jumps.[16] Additionally, H/D exchange is ideally suited as a structural probe for individual BH bonds.[19]

Recently, we showed that the synthesis of $LiBH_4$ is possible under mild conditions (ambient pressure at 390 K) if starting from LiH under gaseous diborane atmosphere. This clearly shows that the formation of BH bonds is the rate limiting step for hydrogen uptake.[20] A better understanding of the BH bond nature and formation is therefore a key parameter for the use of borohydrides as hydrogen storage materials.

We present here the first endeavor of infrared pump−probe (IR-pump−probe) spectroscopy and two-dimensional infrared (2D-IR) spectroscopy on the complex hydride $LiBH_4$. We demonstrate that this spectroscopic method in combination with H/D isotope exchange to $LiB(H_{1-x}\ D_x)_4$ gives insights into the nature of the BH bond that are unaccessible by other methods: anharmonicity, vibrational lifetimes, and homogeneous and inhomogeneous broadening parameters. Furthermore, 2D-IR and IR-pump−probe spectroscopy contain characteristic spectral signatures from Fermi resonances and thermalization processes.

Our approach is a full spectroscopic characterization of $LiBH_4$ at four different isotope-substitution levels: $LiBD_4$, $LiB(H_{0.9}D_{0.1})_4$, $LiB(H_{0.1}D_{0.9})_4$, and $LiBH_4$, employing both linear (FTIR) and nonlinear (IR-pump−probe and 2D-IR) spectroscopy.

Our paper is organized as follows: First, we do a thorough assignment of the vibrational bands of the five different kinds of units appearing in the isotopically diluted hydride BH_4^-, BH_3D^-, $BH_2D_2^-$, BHD_3^-, and BD_4^-, on the basis of FTIR spectra and temperature-difference FTIR spectra. Then, we present the results of 2D-IR spectra and IR-pump−probe spectra on each of the various isotopomers, identifying anharmonicities, vibrational lifetimes, Fermi resonances, and thermalization effects. Finally, we discuss our results and the prospects for extending nonlinear infrared spectroscopic measurements on hydrides.

* To whom correspondence should be addressed. E-mail: phamm@pci.uzh.ch.
[†] Universität Zürich.
[‡] Empa.
[§] ISIS.

10.1021/jp907746z CCC: $40.75
Published on Web 10/09/2009

Methods

Sample Preparation. Bulk $LiBH_4$ and $LiBD_4$ (97% D) were purchased from CatChem, Czech Republic (>98% purity). Isotope-substituted $LiB(H_{0.9}D_{0.1})_4$ and $LiB(H_{0.1}D_{0.9})_4$ samples (200 mg) were obtained by exposing $LiBH_4$ to 2×10^6 Pa D_2 gas pressure at 453 K temperature for 40 min and at 528 K for 36 h, respectively. H−D exchange is monitored by the mass change in a Rubotherm magnetic suspension balance. The samples were handled solely in argon glove boxes for preparation and measured without contact to air. All measurements were performed in transmission on thick films deposited on CaF_2 substrates. For making films, the bulk samples were first diluted in tetrahydrofuran (THF). The filtered saturated solutions were then deposited on 2 mm thick CaF_2 windows and dried at 90 °C in the argon glovebox for 30 min, resulting in 20−60 μm thick films. The CaF_2 window was mounted in Ar in a brass cell, with another CaF_2 window on top, separated by a 6 mm Teflon spacer. It was observed that a sample prepared this way delivers measurable pump−probe signal for several days.

FTIR Spectroscopy. The FTIR measurements were done in transmission between 298 and 358 K with a Bio-Rad 175C FTIR spectrometer. To measure at elevated temperatures, the brass cell containing the sample was mounted in a home-built heater mount, whose temperature was monitored by a thermocouple. All the FTIR measurements were done in nitrogen atmosphere.

***Ab Initio* Calculations.** The normal mode vibrational analysis of $LiBH_4$ and $LiBD_4$ was performed with *ab initio* lattice dynamics based on density-functional theory and the plane-wave pseudopotential method as implemented in the CASTEP code.[21,22] Pseudopotentials were of the optimized norm-conserving variety[23] with a plane-wave cutoff of 450 eV. Calculations were performed under the PBE approximation to exchange and correlation.[24] Brillouin zone integration was performed according to the Monkhorst−Pack scheme with a $2 \times 3 \times 2$ mesh of *k*-points, which gave convergence of all modes to a precision of better than 3 cm^{-1}. Pseudopotential errors in the frequencies were estimated at no more than 1% from a comparison of alternative pseudopotentials. While the structure was fully relaxed on internal geometry, the cell parameters were kept fixed at the experimental room temperature values (a = 7.179 Å, b = 4.437 Å, c = 6.803 Å, taken from ref 25). Relaxed BH distances were 1.220−1.225 Å.

The normal modes of the crystalline phase were determined from dynamical matrices calculated using density-functional perturbation theory (DFPT).[22,26] Infrared tensors were calculated by numerical differentiation of polarization tensors obtained using DFPT, and infrared intensities were calculated using the formalism presented in ref 27. For the mode analysis of partially exchanged $BH_{4-n}D_n^-$, hydrogen atoms were successively replaced by deuterium in the crystalline $LiBH_4$ unit cell. We have considered exchange of the symmetry inequivalent H/D atoms, with all combinations for H-D exchange at 4*c* and 8*d* Wyckoff atomic positions. The slight geometry change induced by deuteration could only be predicted by an anharmonic DFT calculation, which is beyond the scope of this paper.

Infrared Pump−Probe Spectroscopy and 2D-IR Spectroscopy. Details of the theoretical and experimental aspects of infrared pump−probe and 2D-IR spectroscopy can be found elsewhere.[28−30] In brief, the light source is a regeneratively amplified Ti:Sapphire laser operating at 780 nm with a repetition rate of 1 kHz. Two optical parametric amplifiers (OPA1 and OPA2) can be pumped simultaneously, each delivering stable mid-IR pulses which have approximately 1 μJ pulse energy and approximately 100 fs duration fwhm and 150 cm^{-1} spectral width fwhm, which are tunable in the range 3−6 μm.[31] Figure 1 displays the setups for the three different IR-pump−probe methods.

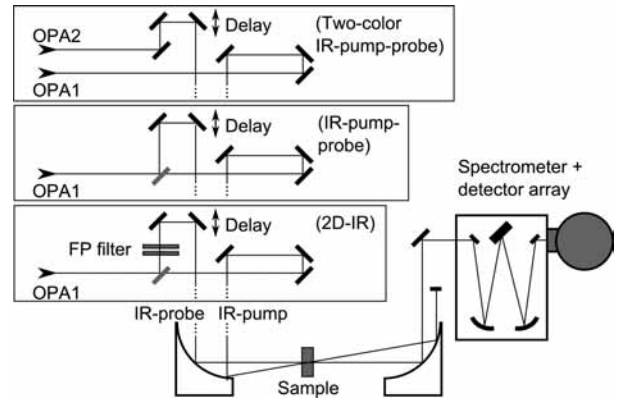

Figure 1. Scheme of the experimental setups used for two-color IR-pump−probe, IR-pump−probe, and 2D-IR spectroscopy. FP filter: Fabry−Perot filter. The IR-pump beam was chopped.

IR-Pump−Probe. IR-pump−probe uses the same broadband IR-pulse for pumping as well as probing. The IR-pump thus excites all modes within the measurement window. The mid-infrared pulses from one OPA are divided into a strong IR-pump pulse and a weak IR-probe pulse, which are spatially overlapped in the sample in the so-called pump−probe geometry. The IR-pump is chopped at half the repetition rate of the laser system, and for each IR-pump−IR-probe delay, a "transient spectrum" is measured as the difference in absorption between the two states IR-pump on and IR-pump off. Measuring transient spectra at a sequence of delays between IR-pump and IR-probe allows one to construct "transient traces" as the signal at one IR-probe frequency versus delay time between pump and probe.

Two-Color IR-Pump−Probe. Two-color IR-pump−probe uses broadband IR-pulses of different wavelengths for pumping and probing. The mid-IR pulse from one OPA is used as the IR-pump, while the IR-probe comes from the other OPA. The remaining details are as in the (one-color) IR-pump−probe experiment described above.

2D-IR. 2D-IR employs a narrow-band IR-pump and a broadband IR-probe; the IR-pump can thus excite a single mode within the measurement window. In effect, the IR-pump−probe setup is employed with the exception that a Fabry−Perot etalon is inserted in the IR-pump beam, which spectrally filters the IR-pump spectrum down to ca. 15 cm^{-1}. The 2D-IR spectrum is obtained by measuring IR-pump−IR-probe spectra for different IR-pump frequencies and composing a two-dimensional intensity plot versus IR-pump and IR-probe frequencies, ν_{pump} and ν_{probe}.

In all measurements, pump and probe pulses were parallely polarized. Furthermore, many separate data sets were acquired, for each of which the delay scheme was perturbed by adding a small random Δt to each delay. The final data set was obtained as an average of these data sets, which served to average out the contribution of interfering scattered pump light with probe light to the signal.

Band Assignments

Phonons in $LiBH_4$ can be well approximated by so-called internal and external vibrations,[9,32] where internal refers to the characteristic vibrations of the BH_4^- ion, and external refers to the vibrational properties of the whole crystal structure. Accordingly, the labeling $\nu_{1,...,4}$ of the internal vibrations is based

TABLE 1: Experimental Stretching Mode Infrared Frequencies [cm^{-1}] for the Various B($H_{4-n}D_n$)$^-$ Units from the Temperature Difference FTIR Spectra Compared to the Theoretical Infrared Frequencies for the Periodic Solid at DFT Level[a]

mode	FTIR frequency	anharmonicity	theory frequency	theory intensity	D sites
		BD_4^-			
$\nu_1(B_{1u}+B_{3u})$	1606[b]		1648	0.26 + 0.13	
$\nu_3'(B_{1u}+B_{3u})$	1736[b]	<19 cm^{-1}	1767−1769	8.04 + 3.74	
$\nu_3(B_{1u}+B_{3u})$	1760[b]		1790−1795	2.02 + 6.58	
$\nu_3''(B_{2u})$	1722[b]		1775	17.18	all
$2\nu_4(B_{1u}+B_{3u})$	1656[b]				
$2\nu_4''(B_{2u})$	1679[b]				
		BHD_3^-			
$\nu_1(B_{1u}+B_{3u})$	1617−1628[b,f,e]		1679	1.83 + 0	$8d + 4c_2$
$\nu_1(B_{1u}+B_{3u})$	1641[e]		1691	1.5 + 0.29	$8d + 4c_1$
$\nu_3'(B_{1u}+B_{3u})$	1738[e]		1771−1773	4.21 + 7.59	$8d + 4c_2$
$\nu_3'(B_{1u}+B_{3u})$	1761[e]		1790−1795	1.64 + 7.03	$8d + 4c_1$
$\nu_3''(B_{2u})$	1722[e]		1775	17.14	$8d + 4c_2$
$\nu_3''(B_{2u})$	1722[e]		1775	17.11	$8d + 4c_1$
$\nu_3(B_{1u}+B_{3u})$	2342[b,f,e]		2351−2354	14.33 + 6.39	$8d + 4c_1$
$\nu_3(B_{1u}+B_{3u})$			2389−2395	9.14 + 6.64	$8d + 4c_2$
$2\nu_4(B_{1u}+B_{3u})$	2258[b,f,e]				
		$BH_2D_2^-$			
$\nu_1(B_{1u}+B_{3u})$			1698	0.96 + 4.48	$4c_1 + 4c_2$
$\nu_1(B_{1u}+B_{3u})$	1664[d,e]		1726−1728	0.12 + 3.5	8d
$\nu_3'(B_{1u}+B_{3u})$	1747[d,e]		1778−1780	8.93 + 0.14	$4c_1 + 4c_2$
$\nu_3''(B_{2u})$	1722[d,e]	57 cm^{-1}	1775	17.1	8d
$\nu_3(B_{1u}+B_{3u})$			2344−2345	5.81 + 11.78	8d
$\nu_3(B_{1u}+B_{3u})$	2276[e]		2383−2385	0.25 + 11.75	$4c_1 + 4c_2$
$\nu_3'(B_{1u}+B_{3u})$	2342[e]		2395−2403	16.43 + 1.96	8d
$\nu_3''(B_{2u})$	2312[e,f]		2390	36.86	$4c_1 + 4c_2$
		BH_3D^-			
$\nu_1(B_{1u}+B_{3u})$	1689[d,g]		1721	5.41 + 2.81	$4c_2$
$\nu_1(B_{1u}+B_{3u})$	1697[d,g]	44 cm^{-1}	1752−1755	3.14 + 2.52	$4c_1$
$\nu_3(B_{1u}+B_{3u})$	2230[d,g]		2340−2343	10.13 + 0.37	$4c_1$
$\nu_3(B_{1u}+B_{3u})$			2363−2365	5.97 + 1.15	$4c_2$
$\nu_3'(B_{1u}+B_{3u})$	2334[g]		2392−2394	4.06 + 16.53	$4c_1$
$\nu_3'(B_{1u}+B_{3u})$	2342[d]		2406−2412	3.6 + 16	$4c_2$
$\nu_3''(B_{2u})$	2306[d]		2390	36.66	$4c_1$
$\nu_3''(B_{2u})$	2306[d]		2390	36.64	$4c_2$
		BH_4^-			
$\nu_1(B_{1u}+B_{3u})$			2325	1.91 + 1.94	
$\nu_3(B_{1u}+B_{3u})$	2276[c,d]		2385 + 2390	16.7 + 7.32	
$\nu_3'(B_{1u}+B_{3u})$	2342[c]		2407 + 2413	3.42 + 13.55	none
$\nu_3''(B_{2u})$	2306[c,d]	<19 cm^{-1}	2390	36.45	
$2\nu_4(B_{1u}+B_{3u})$	2179[c,d]				

[a] Infrared intensities are calculated with the CASTEP LR code in [$(D/A)^2$/amu]. Excited state absorption (ESA) frequencies [cm^{-1}] from the 2DIR pump-probe measurements. D positions after ref 10. [b] Experimental frequencies from the FTIR spectrum of $LiB(H_{0.03}D_{0.97})_4$. [c] Experimental frequencies from the FTIR spectrum of $LiBH_4$. [d] Experimental frequencies from the FTIR spectrum of $LiB(H_{0.90}D_{0.10})_4$. [e] Experimental frequencies from the FTIR spectrum of $LiB(H_{0.35}D_{0.65})_4$. [f] Experimental frequencies from the FTIR spectrum of $LiB(H_{0.10}D_{0.90})_4$. [g] Experimental frequencies from the FTIR spectrum of $LiB(H_{0.95}D_{0.05})_4$.

on the vibrational modes of a free BH_4^- tetrahedral molecule, as the splitting due to the crystal field is small (typically on the order of 1 cm^{-1}). ν_1 and ν_3 are stretching modes while ν_2 and ν_4 are bending modes, following existing nomenclature for methane.[33] Our FTIR assignments are summarized in Table 1.

$LiBD_4$ and $LiBH_4$. For isotopically pure $LiBD_4$ and $LiBH_4$, the BD (BH) stretching region contains 4 stretching modes labeled ν_1, ν_3, ν_3', and ν_3''.[9] The ν_1 mode corresponds to four hydrogen atoms vibrating in phase (symmetric BD or BH stretching mode), while for the ν_3, ν_3', and ν_3'' modes, at least one deuterium (hydrogen) atom vibrates in antiphase with respect to the others (antisymmetric BD or BH stretching). For the case of a fully symmetric BD_4^- (BH_4^-) tetrahedron, the ν_1 mode is not IR active. However, in the crystal, the BD_4^- (BH_4^-) unit is slightly distorted and ν_1 becomes slightly active (see Table 1). The infrared BD stretching of $LiBD_4$ and BH stretching of $LiBH_4$ are displayed in Figure 2a,b, respectively. In parts c and d are the corresponding temperature-difference IR spectra, which serve two purposes: (i) There is improved frequency resolution with respect to absorbance IR spectra (we use here the fact that frequencies of internal modes do not shift by a significant amount with temperature, due to the localized nature of the BH_4^- vibrations, only a broadening occurs).[34] (ii) It will become apparent later that in 2D-IR spectra and IR-pump−probe measurements, the IR-pump heats up the sample, so transient spectra at large delay times are in fact temperature-difference IR absorption spectra. The recording of temperature-difference FTIR spectra facilitates comparison and allows us to establish the temperature jump induced by the IR-pump. In general, we follow the IR assignment proposed by Harvey and McQuacker;[9] we however assigned the main band at 1736 cm^{-1} in $LiBD_4$ to $\nu_3(B_{1u}+B_{3u})$ and not $\nu_3''(B_{2u})$, as new information came from the H−D exchange (see next section).

In $LiBH_4$ the presence of a Fermi resonance between ν_1 and the bending modes complicates somewhat the assignment in the BH stretching region.[11,13,35] Consequently, the ν_1 mode is

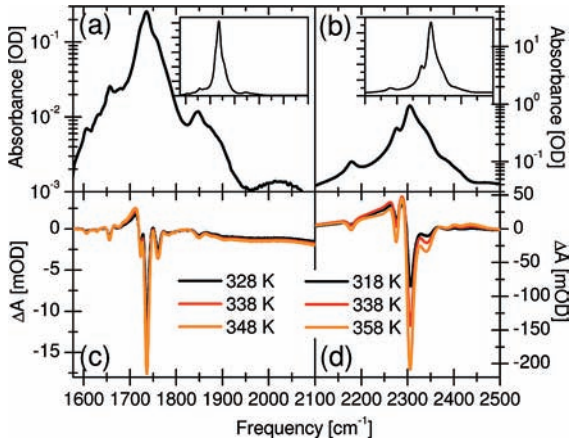

Figure 2. (a) Infrared BD stretching region of $LiBD_4$ (97% D). (b) BH stretching region of $LiBH_4$ at 298 K on a CaF_2 substrate. The insets show the same spectra on a linear scale. (c, d) Corresponding temperature-difference IR spectra with respect to 298 K.

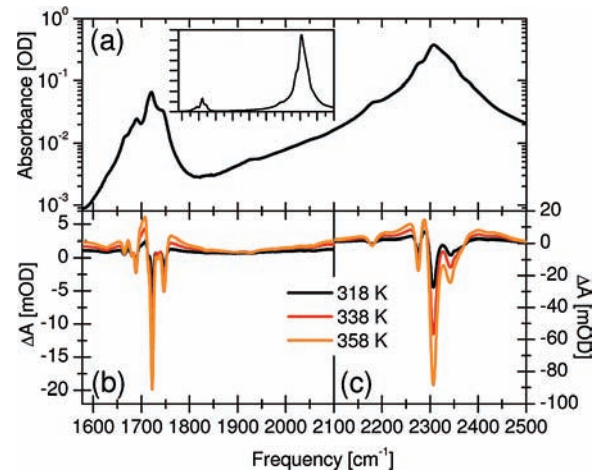

Figure 3. (a) BD and BH stretching regions of the IR spectrum at 298 K. The inset shows the same spectrum on a linear scale. (b, c) Temperature-difference IR spectra with respect to 298 K of a $LiB(H_{0.9}D_{0.1})_4$ film on a CaF_2 substrate.

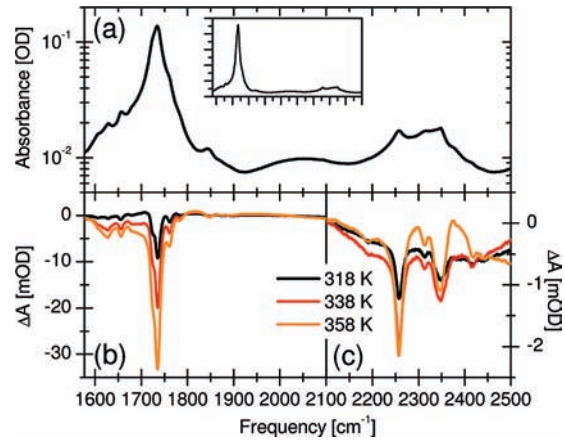

Figure 4. (a) BD and BH stretching regions of the IR spectrum at 298 K. (b, c) Temperature-difference IR spectra with respect to 298 K of a $LiB(H_{0.1}D_{0.9})_4$ film on a CaF_2 substrate.

pushed into the ν_3 region and cannot be distinguished due to to its low intrinsic IR activity. In contrast to ref 9, we assigned the main band at 2306 cm^{-1} to $\nu_3''(B_{2u})$ symmetry, as this is by far the most intense vibration according to the *ab initio* calculation.

H−D Exchange. Due to their large reduced mass difference, vibrational modes mostly involving H atoms (henceforth referred to as BH vibrations) are easily distinguished in the $LiB(H_{1-x}D_x)_4$ infrared spectra from the modes where the D movements dominate (BD vibrations). Furthermore, as two different BH bond lengths exist in the crystal,[10] D-substitution at different sites results in a further splitting of each mode.[18] Exchanging a fraction of the hydrogen in the sample for deuterium results in a partial H−D exchange in the BH_4^- unit and the coexistence of all $BH_{4-x}D_x^-$ ($0 \le x \le 4$) units.[18] The fraction of each $BH_{4-x}D_x^-$ unit in a sample of overall D-fraction x is then determined by a statistical distribution of the units at the exchange temperature, which, however, is biased toward D-rich compounds due to the different zero-point energy of various $BH_{4-n}D_n$ units.[18] The assignments for the BH (BD) stretching modes of each $BH_{4-x}D_x^-$ unit were obtained by comparing the infrared spectra of samples with nominal D-fraction $x = 0$, 0.1, 0.65, 0.9, and 0.97 with each other and with the outcome of the *ab initio* calculation. They are summarized in Table 1. In the following, we will discuss in more detail the two partially H/D exchanged films measured by both FTIR and 2D-IR or IR pump−probe.

$LiB(H_{0.9}D_{0.1})_4$. We showed recently by Raman scattering[18] that the fingerprint for the presence of a particular $BH_{4-x}D_x^-$ unit is the symmetric BD stretching mode $\nu_1(BH_{4-x}D_x^-)$, as these modes are present at regularly spaced frequencies and well-separated from each other. ν_1 modes are much less infrared than Raman active. However, they are still detectable in the H/D exchanged samples, as shown in Figure 3. Here, the coexistence of BH_3D^-, $BH_2D_2^-$, and BHD_3^- is established by the presence of ν_1 absorptions at 1689, 1664, and 1628 cm^{-1}, respectively, in accordance with the corresponding Raman frequencies.[18]

The most active mode in the BD stretch region is an antisymmetric stretching $\nu_3''(B_{2u})$ at 1722 cm^{-1}. We attribute it to the $\nu_3''(B_{2u})$ mode of the $BH_2D_2^-$ unit (calculated frequency: 1775 cm^{-1}), as there is no antisymmetric stretching for the BH_3D^- unit. The analysis of the vibrational amplitudes of this mode reveals that two deuterium atoms move in antiphase with respect to each other, with the two hydrogen atoms almost at rest. This explains why substituting one or two of the remaining hydrogen atoms by deuterium results in the same calculated vibrational frequency of 1775 cm^{-1}, and justifies our assignment of the experimental absorption at 1722 $^{-1}$ of the $LiBD_4$ film to $\nu_3''(B_{2u})$ of the BD_4^- unit.

$LiB(H_{0.1}D_{0.9})_4$. Here, the ν_1 modes reveal the presence of BD_4^- and BHD_3^- units with absorption at 1606 cm^{-1} and 1628 cm^{-1}, respectively, as seen in Figure 4. The ν_3 BD stretching region is similar to the same region in $LiBD_4$, except that absorption bands are broader, an effect that can be attributed to the increased disorder induced by isotope exchange and the presence of the BHD_3^- unit.

In the BH stretching region, only one vibrational $\nu_3(BHD_3^-)$ is expected, split only by the two possible 4c crystallographic sites for the H-atom. Theory predicts a site-splitting of approximately 40 cm^{-1} (calculated frequencies 2350−2390 cm^{-1}). In contrast, the experimental spectra contain two main bands, separated by 90 cm^{-1} at 2258 cm^{-1} and 2342 cm^{-1}, and a small absorption at 2312 cm^{-1}. From comparison with the other partially H−D exchanged samples, we attribute the latter to the $\nu_3''(B_{2u})$ vibration originating from small $BH_2D_2^-$ amounts. The interval between the two main bands is however too large to explain it by site-splitting. A Fermi resonance between the ν_3 BH vibration and the $2\nu_4$ overtone is much more probable, as corroborated by the corresponding 2D-IR measurements (see Vibrational Lifetime section).

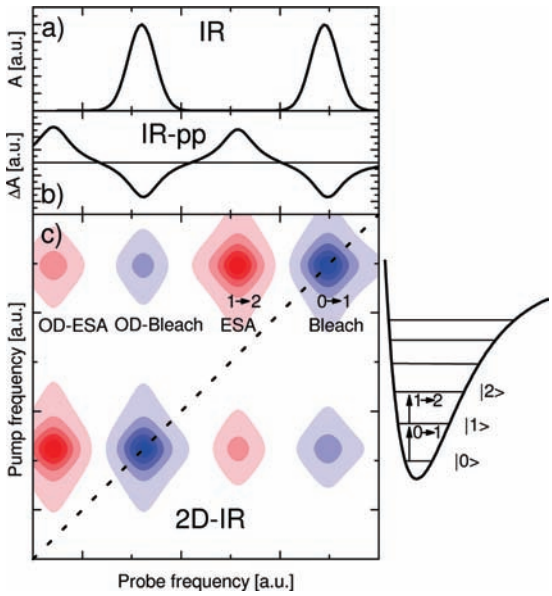

Figure 5. Mutually corresponding sketches of (a) infrared absorption spectrum, (b) IR-pump−probe spectrum, (c) 2D-IR spectrum. See text for discussion of the labels. Blue is negative and red is positive.

IR-Pump−Probe and 2D-IR Spectroscopy

Principles. Before we start, we briefly discuss the information content of a 2D-IR spectrum to facilitate discussion of our results (see Figure 5a−c for visualization of the discussed terms). The action of a narrow-band IR-pump pulse is to selectively excite one particular mode into its first excited state. The subsequent IR-probe pulse will then see two contributions of opposite sign: The bleach of the 0 → 1 absorption, which is a decrease in absorption due to the depletion of the 0-state and the 1 → 0 stimulated emission, due to population in the 1-state which is also seen as a decrease in absorption, and the 1 → 2 excited-state absorption (ESA), seen as an increase in absorption, from the molecules that have been excited by the IR-pump pulse. The bleach/stimulated emission signal and the ESA are generally not located at the same frequency due to anharmonicity, defined as the frequency of the 0 → 1 absorption minus that of the 1 → 2 absorption. They will appear separated in frequency by the anharmonicity which can thus be directly read off from the 2D-IR spectrum. From the transient trace at the frequency of an ESA, the vibrational lifetime can be directly measured. If two modes are within the frequency range of a 2D-IR spectrum, and if these two modes are anharmonically coupled, off-diagonal bleach (OD-bleach) and ESA (OD-ESA) signals will appear in addition. Finally, a 2D-IR spectrum can distinguish between homogenously and inhomogenously broadened bands; a band which is inhomogenously broadened due to a difference in the surroundings seen by individual vibrators will appear elongated along the diagonal in a 2D-IR spectrum.

A broadband pump−probe spectrum (Figure 5b) will include the same signals, however, no longer resolved along the pump-frequency axis since all modes are excited at the same time.

Vibrational Lifetime. In the following, we will report on the measurement of the vibrational lifetimes of the BD and BH vibrations in either isotopically pure samples ($LiBD_4$ and $LiBH_4$), or in isotope diluted samples (the BD vibration in $LiBH_2D_2$ and the BH vibration in $LiBHD_3$). In either case, we use the decay of the ESA signal to deduce the vibrational lifetime, because that is less affected by the heating of the crystal subsequent to vibrational relaxation (see Thermalization section).

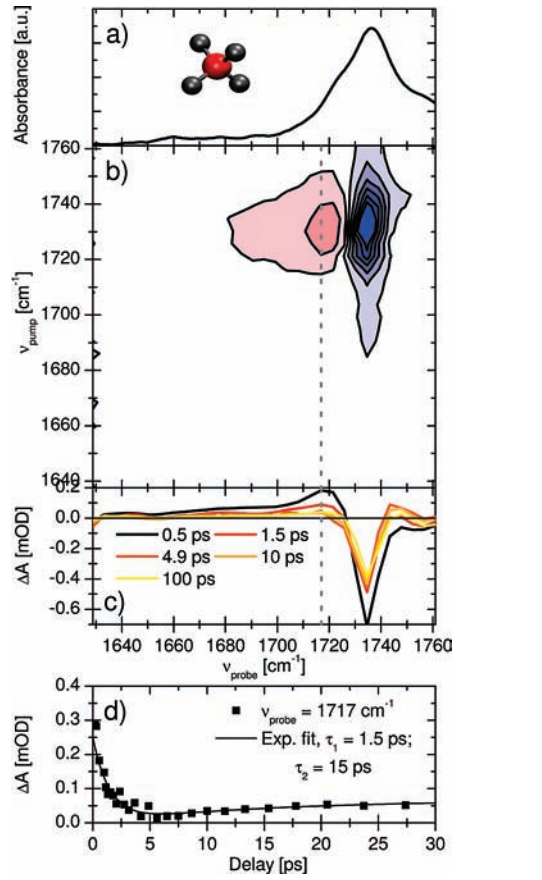

Figure 6. $LiBD_4$: (a) FTIR spectrum, (b) 2D-IR spectrum (blue is negative and red is positive), (c) IR-pump−probe transient spectra, (d) IR-pump−probe transient trace at $\nu_{probe} = 1717$ cm^{-1} (marked by vertical gray, dotted line).

$LiBD_4$ and $LiBH_4$. In order to identify the frequencies of the ESA in BD_4^-, we first acquired its 2D-IR spectrum (Figure 6b). Only the strongest mode, ν_3' at 1736 cm^{-1}, is observed in the 2D-IR spectrum. The peaks in the 2D-IR spectrum show little or no elongation along the diagonal, indicating the absence of any inhomogenous broadening. There is a strong overlap between the bleach and the ESA, so the anharmonicity must be less than the peak−dip separation, i.e., less than 19 cm^{-1}. Nevertheless, the peak at $\nu_{probe} = 1717$ cm^{-1} contains a contribution mainly from the ESA. Figure 6c shows transient spectra from a broadband-pump−probe experiment and Figure 6d the kinetics of the decay of the ESA signal. An excited-state decay time of 1.5 ps is found, when a second exponential is included in the fit to take into account the subsequent thermalization dynamics (see Thermalization section).

IR-pump−probe and 2D-IR measurements were also undertaken for $LiBH_4$ (data not shown). These measurements yielded results similar to those obtained for $LiBD_4$, i.e., a vibrational lifetime of 1.5 ps and a small anharmonicity, comparable to the line width.

$LiB(H_{0.9}D_{0.1})_4$. The spectroscopy is significantly more complex in isotope-diluted samples since mixtures of isotopomers occur (Figure 7a). The strongest signal in the 2D-IR spectrum of $LiB(H_{0.9}D_{0.1})_4$ in the BD region originates from the ν_3'' vibration of $BH_2D_2^-$ at 1722 cm^{-1} (Figure 7b). Statistically, one would expect six times more BH_3D^- units than $BH_2D_2^-$ for a $LiBH_{0.9}D_{0.1}$ sample. However, due to the difference in vibrational zero-point energy between different $BH_{4-n}D_n$ units, the distribution is biased toward D-rich units, resulting in an experimental population ratio of only 1.5.[18] Together with the

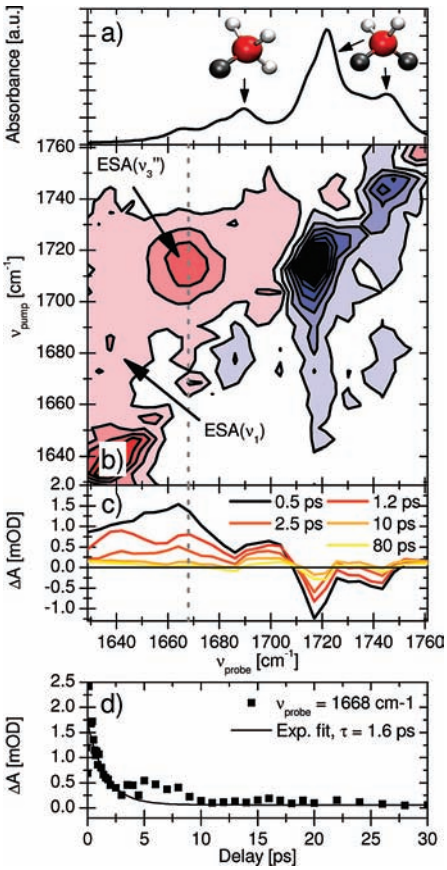

Figure 7. $LiB(H_{0.9}D_{0.1})_4$: (a) FTIR spectrum, (b) 2D-IR spectrum (The excited state absorptions are marked. Blue is negative and red is positive.), (c) IR-pump−probe transient spectra, (d) IR-pump−probe transient trace at ESA(ν_3''), ν_{probe} = 1668 cm^{-1} (marked with vertical gray, dotted lines).

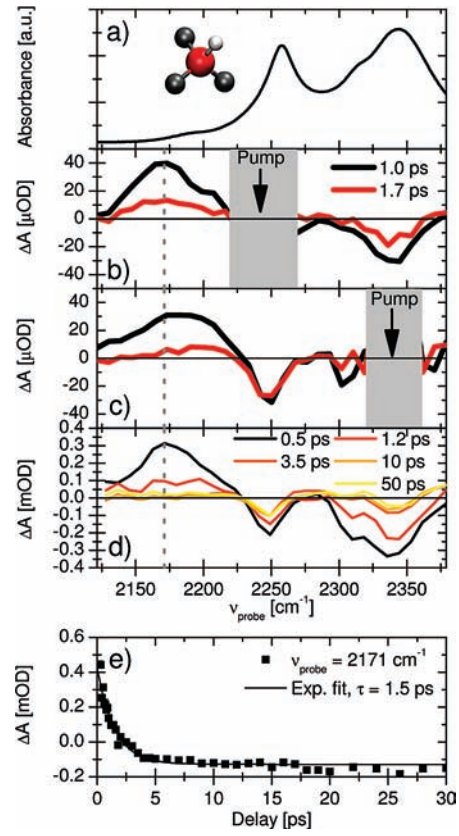

Figure 8. $LiB(H_{0.1}D_{0.9})_4$: (a) FTIR spectrum, (b) horizontal slice of the 2D-IR spectrum with ν_{pump} = 2250 cm^{-1}, (c) horizontal slice of the 2D-IR spectrum with ν_{pump} = 2336 cm^{-1} (grey rectangles have been added to conceal scattered IR-pump light), (d) IR-pump−probe transient spectra, (e) IR-pump−probe transient trace at ν_{probe} = 2171 cm^{-1} and exponential fit.

higher intensity of the ν_3'' vibration of $BH_2D_2^-$, as predicted from the DFT calculation (see Table 1), this qualitatively explains the dominance of this band.

The corresponding ESA is found at 1665 cm^{-1} (ESA(ν_3'')) revealing an anharmonicity of 57 cm^{-1}. Again, these peaks are not elongated along the diagonal, indicating the absence of any inhomogenous broadening. Also, ν_3 of $BH_2D_2^-$ at 1747 cm^{-1} can readily be identified in the 2D-IR spectrum, while its ESA cannot be clearly assigned due to the overlap with the strong ν_3'' band. Less clear is ν_1 of BH_3D^- at 1689 cm^{-1}. Probably, the ESA of this band is at 1635 cm^{-1} (ESA(ν_1)), revealing an anharmonicity of 44 cm^{-1}. It should be noted that there seems to be an OD-bleach pertaining to this band, appearing at ν_{probe} ≈1747 cm^{-1}. In analogy to the BH vibration of BHD_3^- (see discussion in the next paragraph), where this feature is more evident, we assign it to a Fermi resonance with the BD bend vibration.

Again, a vibrational lifetime of 1.5 ps is obtained from an single exponential fit of the broad IR-pump−probe response, which is dominated by the ν_3'' vibration of $BH_2D_2^-$ (Figure 7c,d).

LiB(H$_{0.1}$D$_{0.9}$)$_4$. The spectrum of $LiB(HD_{0.1}D_{0.9})_4$ in the BH region is dominated by two bands at 2258 and 2342 cm^{-1}, both of which have been assigned to the BH vibration of BHD_3^- (Figure 8b,c). The sample was highly scattering, and we could only measure slices through a 2D-IR spectrum with the pump-frequency tuned to these two bands (Figure 8b,c). In both cases, we see a positive peak at ca. 2170 cm^{-1}. In addition, we observe OD-bleaches at ca. 2342 cm^{-1} in Figure 8b and ca. 2258 cm^{-1} in Figure 8c that reveal the presence of anharmonic coupling between the two bands. The observation of a cross peak rules out the possibility that the two bands belong to the same mode in separate BHD_3^- units at crystallographically different sites. Given the early delays at which the measurements were done, we can also rule out that the signal has contribution from the thermalization signal (see Thermalization section). We favor the explanation that these cross peaks have their origin in a Fermi resonance. It is known that BH stretching vibrations in BH_4^- are influenced by a Fermi resonance with BH bending modes,[35,36] and indeed the ν_4 bending mode is observed at 1126 cm^{-1} in $LiBH_{0.1}D_{0.9}$ (data not shown). Also, for $-CH_3$ groups, the existence of a Fermi resonance between stretching and bending modes is very well established.[37] The appearance of a Fermi resonance in a 2D-IR spectrum has been studied in detail (see Figure 3b of ref 38), giving rise to exactly the response we observe here. This explanation would also explain the apparent lack of an ESA for the 2342 cm^{-1} band.

Transient pump−probe spectra are presented in Figure 8d, and the transient trace at ν_{probe} = 2171 cm^{-1} (Figure 8e) reveals a vibrational lifetime of 1.5 ps for the BH vibration of BHD_3^-, the same value as observed for BD vibrations.

Thermalization. Subsequent to vibrational relaxation out of the BH or BD vibrations, the deposited energy will eventually heat up the crystal. We already know from the temperature difference spectra of Figure 2b,c, Figure 3b,c, and Figure 4b,c that the absorption spectra respond quite strongly to temperature. In the time-resolved data of the isotopically pure $LiBD_4$ (Figure 6c) we found that while the ESA decays completely within the vibrational lifetime of 1.5 ps, the bleach signal decays only partially and then stays approximately constant until 100 ps (and

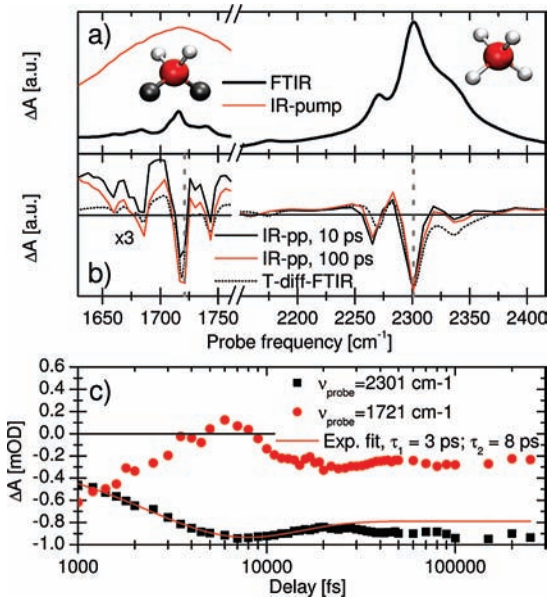

Figure 9. $LiB(H_{0.9}D_{0.1})_4$, with IR-pump at 1700 cm^{-1}: (a) FTIR spectrum and IR-pump spectrum, (b) transient spectra at 10 and 100 ps delay and temperature-difference FTIR spectra, (c) representative transient traces at $\nu_{probe} = 2301$ and 1721 cm^{-1} (marked with vertical gray, dotted lines).

beyond, data not shown). In the isotope-diluted sample, in contrast (Figure 7c), the decay of the long delay time signal is more complete (but still not 100%). It turns out that the long time signal reflects the overall heating of the bulk crystal after dissipating the energy we had deposited in the crystal through the pump pulse. This is evidenced in Figure 9b, where IR-pump−probe transient traces are compared with temperature-difference FTIR spectra of the same sample. Apart from an overall scaling factor, both are essentially identical. The scaling factor can be used to estimate the temperature jump we achieve in the pump−probe experiment, revealing ≈1 K in the case of $LiB(H_{0.9}D_{0.1})_4$ and 6 K in the cases of $LiBD_4$ and $LiBH_4$. In the isotopically pure sample (Figure 6c), vibrational excitation of a BD vibration leads to a heating of all molecules of the same kind, i.e. a comparably large heat signal. In the isotope-diluted sample, in contrast, a significant part of the pump energy heats BH vibrations; consequently, the heat response of the BD vibration is correspondingly weaker (Figure 7c).

The latter conclusion suggests an experiment in which we can disentangle the kinetics of vibrational relaxation (1.5 ps) from that of thermalization of the energy. That is, if we pump the BD vibration of $BH_2D_2^-$, and probe the BH vibration of BH_4^-, all in a $LiB(H_{0.9}D_{0.1})_4$ sample, then we observe directly the dissipation of energy among units. At the same time, we want to avoid pumping and probing BD and BH vibrations, respectively, of the same species, because in this case the result could be affected by anharmonic coupling within one unit. Although the spectra of $LiB(H_{0.9}D_{0.1})_4$ are completely resolved in neither the BD nor the BH spectral regions, we have seen that the dominating contribution in pumping the BD vibration originates from $BH_2D_2^-$ (Figure 7), whereas the spectrum in the BH region is dominated by BH_4^-. Hence, the response of a BD-pump−BH-probe experiment will essentially reflect interunit energy transport and will only to a minor extent be affected by intraunit coupling.

In Figure 9c, the black squares show the appearance of the strongest band in the BH region after pumping BD. A fit of the initial rise of that signal reveals a time constant of 3 ps (when taking also the subsequent dynamics into account in the fit), and the dominating part of the spectral changes are finished within the first 10 ps. A closer inspection of the transient spectra, however, shows that relatively minor band shifts continue to occur until ≈100 ps. These are manifested in the transient spectra (Figure 9c) as small modulations and are visible in both the BD- and BH-stretching regions. Hence, while energy randomizes and dissipates among states within less than 10 ps, complete thermalization among all degrees of freedom of the system takes ≈100 ps. The modulations in the transient traces may be caused by the redistribution of population between low-frequency librations and external modes, which have slightly different anharmonic couplings to the BH vibrations, giving rise to what appear to be oscillations on a logarithmic time scale.

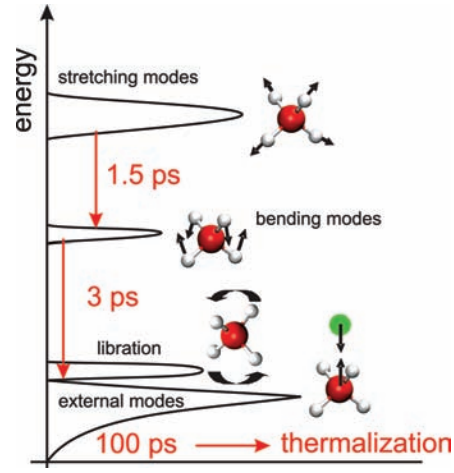

Figure 10. Sketch of the various steps and time constants in vibrational relaxation of $LiBH_4$.

Discussion and Outlook

We have measured the vibrational lifetime of BH and BD vibrations in $LiBH_4$ and various of its isotopomers. The lifetime is ≈1.5 ps and does not depend on isotope constitution within experimental error. For the isotope pure samples, resonant energy transfer mediated by the crystal field (which, however, is very small) could occur, which would result in an anisotropy decay. This, in turn, might affect the transient kinetics, since we used parallel polarizations for pump and probe pulses. However, as we observe the same time constant also in the isotope diluted samples, for which resonant energy transfer should be strongly suppressed,[39] we conclude that this effect is not very prominent.

Typical vibrational relaxation times of molecules in the solution phase (for which significantly more reference values exist) lie between ca. 1 ps and a few tens of picoseconds, depending on the extent to which a particular mode is spectrally isolated.[40] For molecular crystals, lifetimes have predominantly been measured at low temperatures, where generally vibrational lifetimes from picoseconds to a few hundreds of picoseconds are found.[41] In view of this comparison, the 1.5 ps vibrational lifetime we observe in $LiBH_4$ is not unusual, though relatively fast given the small size of the BH_4^- unit and the spectral isolation of the vibrational bands.

In addition, we have investigated the subsequent vibrational energy redistribution and thermalization process. We propose a model which includes three types of modes (Figure 10): the BH or BD stretching modes, which are the ones we excite in the experiment, the low frequency external modes (librational and translational), and the BH or BD bending modes in between.

These different kinds of modes are well-separated in frequency, as shown, e.g., by Raman spectroscopy.[9] After thermalization, only the external modes can be excited, since both stretching and bending modes have frequencies $\gg k_B T$. Nevertheless, we find already after 10 ps (with a time constant of 3 ps) a response that very closely resembles that of a fully thermalized sample (Figure 9). Hence, we conclude that vibrational energy reaches the external modes within 3 ps, albeit not yet in a fully thermalized manner, as evidenced by the persisting modulations of the transient spectra up to $\approx$100 ps.

Interestingly, energy decays out of the originally pumped BH and BD vibration on a time scale faster (1.5 ps) than the appearance in the external modes (3 ps); hence, energy cascades down through some intermediate states. The only possibility for these intermediate states are the BH (BD) bending modes lying around 1100 cm^{-1} (800 cm^{-1}). This interpretation is supported by the existence of strong Fermi resonances between stretching and bending modes, facilitating the fast exchange of energy. In turn, once bending vibrations are excited, they might couple very strongly to librational (hindered rotational) modes of the BH_4^- units which are strongly interlocked among each other in a gearlike fashion.[10]

Maybe not surprisingly for a crystal lattice, we do not find any indication for inhomogeneous broadening in the 2D-IR spectra. On the other hand, temperature has a very strong effect on the line-shape of the BH and BD stretching modes. Consequently, temperature induced disorder does exist which however must fluctuate on very fast time scales so that it gives rise to homogeneous rather than inhomogeneous broadening. In Figure 6, the size of the bleach of the ν_3 mode after direct pumping is about the same as after heating the sample by 6 K. Hence, the coupling of the BD stretching modes to thermally excited external modes must be exceptionally strong, a conclusion that is in accordance with recent studies which found strong anharmonicity of external modes.[13,42] The only mechanism we can imagine at this point for such a strong coupling is hindered rotational degrees of freedom (librations), in analogy to ref 43. We will test this hypothesis in future work.

Furthermore, we determined the anharmonicities of various BH and BD stretch modes. The measured anharmonicities can be related to the cubic and quartic expansion coefficients of the potential energy surface in a straightforward manner.[29,30] The greater anharmonicity in isotope-diluted hydrides facilitates their unambiguous measurement, which is relevant if one wants to use them as a benchmark for *ab initio* calculations. Eventually, the application of these materials for hydrogen storage purposes requires the dissociation of the BH bond and release of molecular hydrogen. The dissociation energy is manifested to a certain extent already in the anharmonicity around the potential energy minimum.

Finally, we completed the assignment of the stretching vibrations for all five different isotopically different $BH_{4-x}D_x^-$ units, aided by temperature-difference FTIR and 2D-IR spectra, and *ab initio* infrared intensity calculations. A consistent analysis is made possible by the *ab initio* calculation of intensities and the comparison of the FTIR spectra of different $BH_{4-x}D_x^-$ units. This led to the revision of the assignment of certain modes. The symmetry breaking induced by H/D exchange within the BH_4^- unit enhances the intensity of the symmetric stretching modes (ν_1) significantly and enables a direct comparison with Raman spectra,[18] where these modes are always very active. Furthermore, partial H/D exchange helps studying individual BH bonds, as exemplified by our finding a new Fermi resonance between bending and stretching vibrations of the BHD_3^- unit.

In conclusion, we have established the time scales of the fastest possible dynamics in metal hydrides using femtosecond IR-pump−probe and 2D-IR measurements. This, together with our measuring anharmonicities and our establishing that the vibrational bands are purely homogenously broadened, represents new insights into the nature of the BH (BD) bond. Future directions for this work could be to extend the measurements to HT-phases of metal hydrides, or to add polarization-sensitivity to the measurement, which would yield information on orientational and rotational dynamics, as well as processes of resonant energy transport. Finally, one could initiate the phase transition between, e.g., the LT and the HT phases by a temperature jump within a few tens of picoseconds, and study its structural transition in great detail.

Acknowledgment. This work was funded by the Swiss National Science Foundation, by the Swiss federal office for Energy via the CompHy project, and by the European Commission, Contract MRTN-CT-2006-032474 (Hydrogen). Computing resources provided by the U.K. e-Science Centre, STFC (SCARF), are gratefully acknowledged. E.R.A. acknowledges financial support through a postdoctoral grant from the Danish Natural Science Research Council.

References and Notes

(1) Schlapbach, L.; Züttel, A. *Nature* **2001**, *414*, 353.
(2) Züttel, A.; Wenger, P.; Rentsch, S.; Sudan, P.; Mauron, P.; Emmenegger, C. *J. Power Sources* **2003**, *118*, 1.
(3) Orimo, S.; Nakamori, Y.; Kitahara, G.; Ohba, N.; Towata, S.; Züttel, A. *J. Alloys Compd.* **2005**, *404*, 427.
(4) Friedrichs, O.; Buchter, F.; Borgschulte, A.; Remhof, A.; Zwicky, C.; Mauron, P.; Bielmann, M.; Züttel, A. *Acta Mater.* **2009**, *60*, 753.
(5) Mauron, P.; Buchter, F.; Friedrichs, O.; Remhof, A.; Bielmann, M.; Zwicky, C. N.; Züttel, A. *J. Phys. Chem. B* **2008**, *112*, 906.
(6) Kostka, J.; Lohstroh, W.; Fichtner, M.; Hahn, H. *J. Phys. Chem. C* **2007**, *111*, 14026.
(7) Yin, L.; Wang, P.; Fang, Z.; Cheng, H. *Chem. Phys. Lett.* **2008**, *450*, 318.
(8) Matsuo, M.; Takamura, H.; Maekawa, H.; Li, H.-W.; Orimo, S. *Appl. Phys. Lett.* **2008**, *94*, 084103.
(9) Harvey, K.; McQuaker, N. *Can. J. Chem.* **1971**, 3282.
(10) Buchter, F.; Łodziana, Z.; Mauron, P.; Remhof, A.; Friedrichs, O.; Borgschulte, A.; Züttel, A. *Phys. Rev. B* **2008**, *78*, 094302.
(11) Gomes, S.; Hagemann, H.; Yvon, K. *J. Alloys Compd.* **2002**, *346*, 206.
(12) Hagemann, H.; Gomes, S.; Renaudin, G.; Yvon, K. *J. Alloys Compd.* **2004**, *363*, 126.
(13) Racu, A.-M.; Schoenes, J.; Łodziana, Z.; Borgschulte, A.; Zuttel, A. *J. Phys. Chem. A* **2008**, *112*, 9716.
(14) Tsang, T.; Farrar, T. C. *J. Phys. Chem.* **1969**, *50*, 3498.
(15) Remhof, A.; Gremaud, R.; Buchter, F.; Łodziana, Z.; Ramirez-Cuesta, A. J.; Borgschulte, A.; Züttel, A. *Z. Phys. Chem.*, in press.
(16) Corey, R. L.; Shane, D. T.; Bowman, R. C.; Conradi, M. S. *J. Phys. Chem. C* **2008**, *112*, 18706.
(17) Shane, D. T.; Bowman, R. C.; Conradi, M. S. *J. Phys. Chem. C* **2009**, *113*, 5039.
(18) Gremaud, R.; Łodziana, Z.; Hug, P.; Willenberg, B.; Racu, A.-M.; Schoenes, J.; Ramirez-Cuesta, A. J.; Clark, S. J.; Refson, K.; Züttel, A.; Borgschulte, A. *Phys. Rev. B* **2009**, *80*, 100301.
(19) Hagemann, H.; D'Anna, V.; Carbonniere, P.; Bardaji, E. G.; Fichtner, M. *J. Phys. Chem. C*, submitted.
(20) Friedrichs, O.; Borgschulte, A.; Kato, S.; Buchter, F.; Gremaud, R.; Remhof, A.; Züttel, A. *Chem.—Eur. J.* **2009**, *15*, 5531.
(21) Clark, S. J.; Segall, M. D.; Pickard, C. J.; Hasnip, P. J.; Probert, M. J.; Refson, K.; Payne, M. C. *Z. Kristallogr.* **2005**, *220*, 567.
(22) Refson, K.; Clark, S. J.; Tulip, P. R. *Phys. Rev. B.* **2006**, *73*, 155114.
(23) Lee, M. H. Ph.D Thesis, Cambridge, 1995.
(24) Perdew, J. P.; Burke, K.; Ernzerhof, M. *Phys. Rev. Lett.* **1996**, *77*, 3865.
(25) Soulié, J.-P.; Renaudin, G.; Cerný, R.; Yvon, K. *J. Alloys Compd.* **2002**, *346*, 200.
(26) Baroni, S.; de Gironcoli, S.; Corso, A. D.; Giannozzi, P. *Rev. Mod. Phys.* **2001**, *73*, 515.
(27) Porezag, D.; Pederson, M. R. *Phys. Rev. B.* **1996**, *54*, 7830.
(28) Woutersen, S.; Hamm, P. *J. Phys.: Condens. Matter* **2002**, *14*, xxxx.

(29) Golonzka, O.; Khalil, M.; Demirdöven, N.; Tokmakoff, A. *Phys. Rev. Lett.* **2001**, *86*, 2154.
(30) Khalil, M.; Tokmakoff, A. *Chem. Phys.* **2001**, *266*, 213.
(31) Hamm, P.; Kaindl, R. A.; Stenger, J. *Opt. Lett.* **2000**, *25*, 1798.
(32) Porto, S. P. S.; Scott, J. F. *Phys. Rev.* **1967**, *157*, 716.
(33) Herzberg, G. *Molecular Spectra and Molecular Structure. II Infrared and Raman Spectra of Polyatomic Molecules*; Van Nostrand Reinhold: New York, 1945.
(34) Borgschulte, A.; Züttel, A.; Hug, P.; Racu, A.-M.; Schoenes, J. *J. Phys. Chem. A* **2008**, *112*, 4749.
(35) Carbonniere, P.; Hagemann, H. *J. Phys. Chem. A* **2006**, *110*, 9927.
(36) Memon, M. I.; Sherman, W. F.; Wilkinson, G. R. *J. Mol. Struct.* **1984**, *115*, 213.
(37) Lavalley, J.; Sheppard, N. *Spectrochim. Acta* **1972**, *28A*, 2091.
(38) Edler, J.; Hamm, P. *J. Chem. Phys.* **2003**, *119*, 2709.
(39) Woutersen, S.; Bakker, H. J. *Nature* **1999**, *402*, 507–509.
(40) Owrutsky, J. C.; Raftery, D.; Hochstrasser, R. M. *Annu. Rev. Phys. Chem.* **1994**, *45*, 519.
(41) Schosser, C.; Dlott, D. *J. Chem. Phys.* **1984**, *80*, 1394.
(42) Hagemann, H.; Filinchuk, Y.; Chernyshov, D.; van Beek, W. *Phase Transitions* **2009**, *82*, 344.
(43) Kriegl, J.; Nienhaus, K.; Deng, P.; Fuchs, J.; Nienhaus, G. *Proc. Natl. Acad. Sci. U.S.A.* **2003**, *100*, 7069.

JP907746Z